applied sciences

MDPI

Article

Analysis of the Design of Henry Muncaster's Two-Cylinder Compound Vertical Steam Engine with Speed Control

José Ignacio Rojas-Sola [1,*] and José Francisco Gutiérrez-Antúnez [2]

[1] Department of Engineering Graphics, Design and Projects, University of Jaen, 23071 Jaen, Spain
[2] Higher Polytechnic School, University of Jaen, 23071 Jaen, Spain
* Correspondence: jirojas@ujaen.es; Tel.: +34-953-212452

Abstract: This article offers an analysis, from the mechanical engineering viewpoint, of an invention by Henry Muncaster from 1912: the two-cylinder compound vertical steam engine with speed control. This is an invention with a large number of components (106) that was used as an engine in boats and railways. The ultimate objective of this investigation was to determine the operating conditions (maximum pressures of water vapor in the admission of high- and low-pressure cylinders) according to the criteria of resistance of materials since there is no information about this. Therefore, two critical operating conditions were simulated that resemble the start-up of the machine (flywheel locked as the most unfavorable situation) in order to determine those operating conditions that ensure both its safety and optimal operation. For this, a static linear analysis based on the finite element method (FEM) of the 3D CAD model was carried out under real operating conditions, according to the criteria of resistance of materials, using the Autodesk Inventor Nastran 2023 software. The results of the static linear analysis (von Mises stress, displacement and safety factor) confirmed the maximum values of the vapor pressure in the admission of the cylinders: 0.3 MPa on the high-pressure piston plunger and 0.15 MPa on the low-pressure piston plunger.

Keywords: Henry Muncaster; steam engine; two-cylinder compound vertical engine; Autodesk Inventor Nastran; computer-aided engineering; finite element analysis

Citation: Rojas-Sola, J.I.; Gutiérrez-Antúnez, J.F. Analysis of the Design of Henry Muncaster's Two-Cylinder Compound Vertical Steam Engine with Speed Control. *Appl. Sci.* **2023**, *13*, 9150. https://doi.org/10.3390/app13169150

Academic Editors: Adrian Irimescu and Wei Li

Received: 16 July 2023
Revised: 2 August 2023
Accepted: 9 August 2023
Published: 11 August 2023

1. Introduction

Steam engines were a milestone in the technological development of the 18th and 19th centuries since water vapor was the most widely used energy. In these machines, steam expands in a cylinder, transforming heat energy into mechanical energy (work). Thus, these are thermal machines which perform work and whose magnitude depends on the gradient between the intake temperature and the exhaust temperature [1,2].

Performing a brief historical review, we note that the first inventors to put this steam engine into service were Papin, Savory and Newcomen. Humphrey Potter developed the automatic operation of the valves; James Watt [3] invented the separate condenser; and Trevithick, Hedley and Hackworth were the pioneers of the locomotive. Thus, as can be seen, its main use was as the engine of different means of locomotion, such as railways or ships, having undergone modifications over time to improve its efficiency and economy. Furthermore, and given the interest of the subject, some of these steam engines have been analyzed from the point of view of engineering graphics [4] and computer-aided engineering [5].

Henry Muncaster was an English engineer with extensive experience in steam engines who applied his knowledge in different industrial sectors, such as mining, coal and steel, among others [6]. In addition, this experience was reflected in numerous articles in the Model Engineer magazine; in 1912, he wrote a small monograph on stationary models powered by steam [7].

The research presented in this article is analyzed from the standpoint of the mechanical engineering one of his inventions, particularly the two-cylinder compound vertical steam

engine with speed control. This research is part of a broader investigation that pursues the objective of conducting an in-depth analysis of each of Henry Muncaster's inventions (an article on another invention was recently published [8]).

Furthermore, in order to carry out the present analysis, the 3D CAD model of the invention [9] was obtained from the graphic documentation (plans) drafted by Julius de Waal [10], outlining the detailed operation of the device.

Edgar T. Westbury [11] defined the invention as highly suitable for use as an engine for powerful ships, tugboats and fast ocean liners. He also commented that the assembly of this engine required careful positioning of the pillars, both at the end of the bedplate and at the flange of the cylinder base, as well as a precise alignment of the sliding bars so that they were parallel to the axis of the cylinder, both transversely and laterally [10].

Moreover, there is no worldwide study from the point of view of the engineering of this engine which underlines its significance, novelty, originality and scientific interest. For this reason, the ultimate goal of this study was to discover the operation conditions (maximum pressures of the water vapor in the admission of the high- and low-pressure cylinders) according to the criteria of the resistance of the materials, since there is currently no information about them. To achieve this, a static linear analysis was conducted [12] of the two-cylinder compound vertical steam engine with speed control, using the finite element method [13] under real operating conditions in order to determine whether it was properly designed and to confirm the maximum values of the vapor pressure in the intake of the high- and low-pressure cylinders. FEM was used because it is not possible to solve the differential equations exactly that govern the problem; thus, this is the reason why we used this method used. This method allows us to divide the continuous medium into a discreet medium, dividing it into small finite elements; then, the variables are calculated in specified points of the medium. These points are the vertices (nodes) of the finite elements. In this way, this method allows us to obtain an approximate solution to the real one if the differential equations could be solved.

The remainder of the paper is structured as follows: Section 2 shows the materials and methods (including its operation) used in this research; then, Section 3 includes the main results and discussion; and Section 4 shows the main conclusions.

2. Materials and Methods

The starting material for the present investigation consisted solely of the graphic documentation (plans) developed by Julius de Waal [10]. From these plans, a 3D CAD model was obtained that is as reliable as the real model, thanks to the Autodesk Inventor Professional 2023 software [14], and different static linear analyses were subsequently performed using the Autodesk Inventor Nastran 2023 [15] software.

On the other hand, as the detailed operation of the invention was published previously [9], in the present article, this operation is described only briefly in order to situate the reader. The different subsections are outlined below.

2.1. Operation of the Machine

In Figure 1, two isometric views of the machine are shown together, along with the name of the most notable elements of the invention. This figure shows two cylinders, a high-pressure and low-pressure cylinder, expanding the working fluid (water vapor) in two stages. Thus, a greater thermal efficiency is achieved, and, in addition, the von Mises stresses are lower since the pressure and temperature gradient in each cylinder is less than in the case of fully expanding up to the atmospheric pressure in a single cylinder.

First, the steam enters through the throttle valve housing. This throttle valve through the control rod of the speed regulator, or governor, modifies the cross-section of the passage of the fluid, that is, the inlet flow. Next, the steam enters the high-pressure cylinder and expands to a certain pressure, ending its expansion to atmospheric pressure in the low-pressure cylinder.

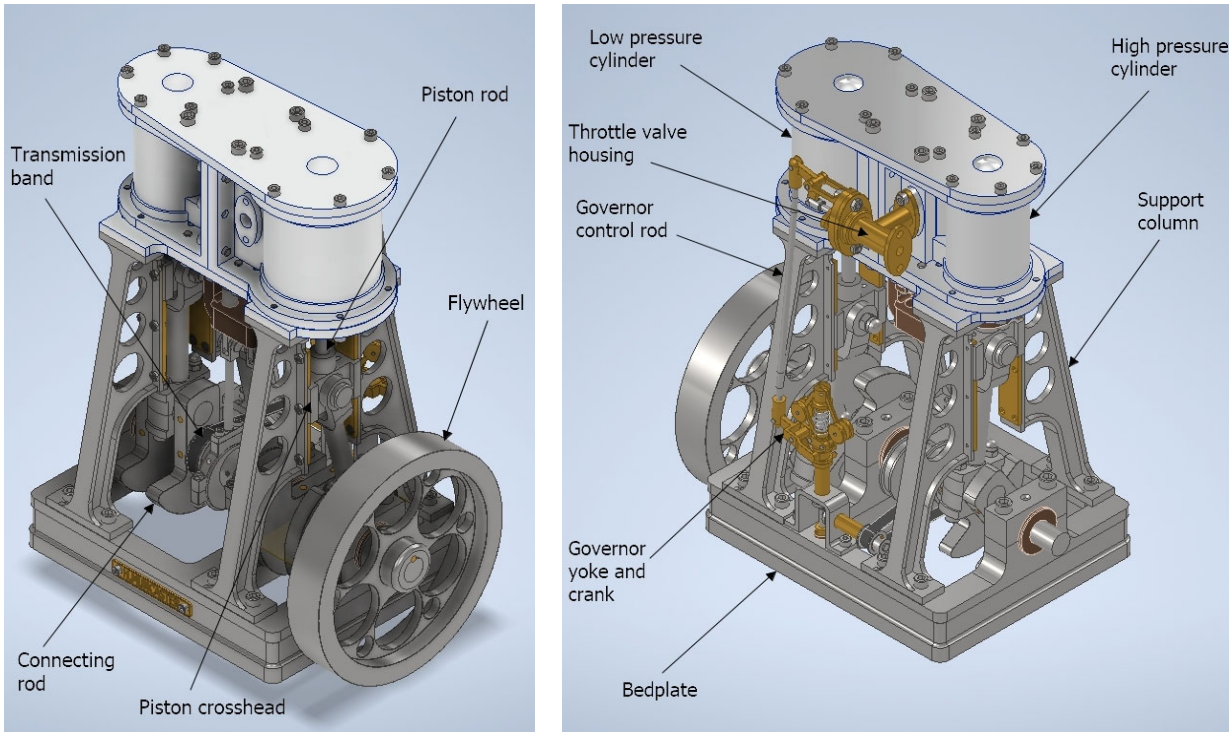

Figure 1. Isometric views of the machine: front view (**left**) and rear view (**right**).

The intake and exhaust of each of the cylinders are produced through slide valves that present an alternative movement, transmitted by an eccentric pulley that rotates at the same angular speed as the crankshaft.

On the other hand, the angular movement of the crankshaft axis is transmitted to the governor horizontal axis through a transmission belt, and this, in turn, transmits the rotation towards the governor vertical axis by means of two gears. The governor also has a sliding collar that compresses the spring and modifies the radius of the trajectory described by the counterweights of the governor. In this way, if the governor control rod is moved, the sliding collar moves upwards, compressing the spring and, in turn, modifying the flow.

Figure 2 shows an isometric view of the subassembly formed by the crankshaft and the elements that have an alternative movement, that is, the pistons and high- and low-pressure slide valves.

Finally, Figure 3 shows a front view of the speed regulator subassembly, together with the names of its most important components.

2.2. Analysis from the Mechanical Engineering Standpoint

This section explains all the stages of the process followed in carrying out an analysis using the finite element method, as well as all the established working hypotheses. The stages are as follows: preprocessing, assignment of materials, application of contacts, boundary conditions, discretization, critical positions, determination of the strain envelope and analysis execution.

2.2.1. Preprocessing

Regarding the subsequent static linear analysis and given the high number of components (106) of the invention, it is appropriate to obtain a simplified model in order to reduce the computational cost and the simulation time.

Furthermore, in order to be able to exclude certain components from the analysis, it must be previously ensured that their presence or absence in the execution of the analysis does not influence the results; that these analyses can be performed separately; or simply

that it does not make sense to analyze them under static load, that is, to perform a static linear analysis.

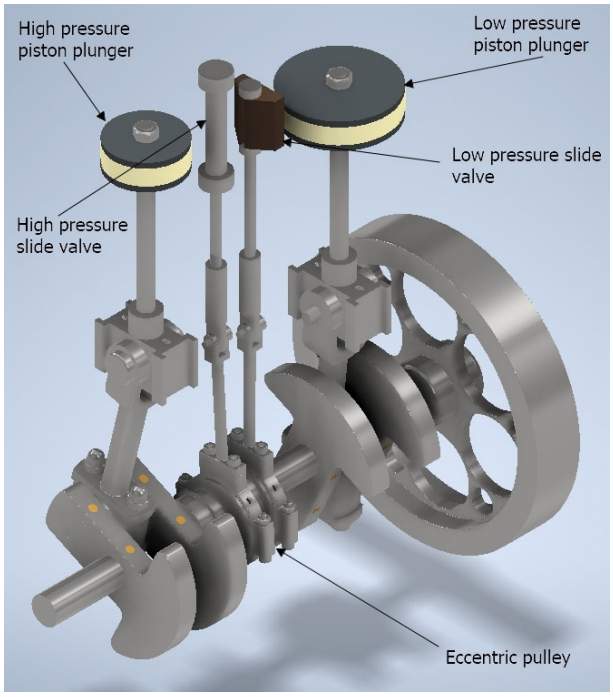

Figure 2. Isometric view of the crankshaft and elements with reciprocating movement.

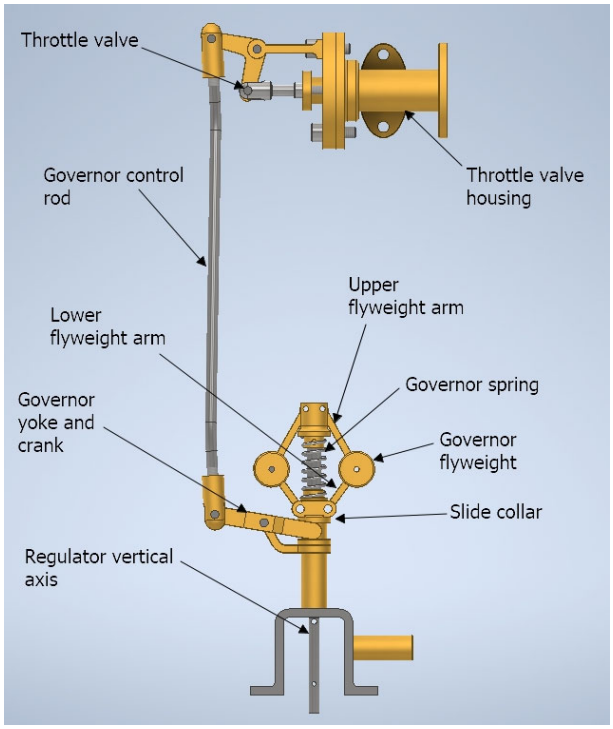

Figure 3. Front view of the speed regulator subassembly.

Thus, the components excluded from the analysis and the reasons for their exclusion are as follows:

- The fixing elements were excluded since they require a very fine mesh size and because there is a large number of this type of component. Thus, some of these elements (bolts

and nuts) are replaced by a 'bonded' contact relationship, that is, by a welded joint. However, it must be taken into account that a welded connection is more rigid than a connection using bolts and nuts, so if critical stress values occur in an area where a fastening element should go or in the contact area, then those initially excluded elements must be included.

- The centrifugal speed regulator was excluded since its operation is basically dynamic, so it does not make any sense to carry out a static linear analysis of this subset. In addition, the critical conditions to be simulated are from the machine stop or start-up conditions, for which the centrifugal speed regulator does not have any angular velocity.

Figure 4 shows two isometric views of the final assembly after excluding the components mentioned above.

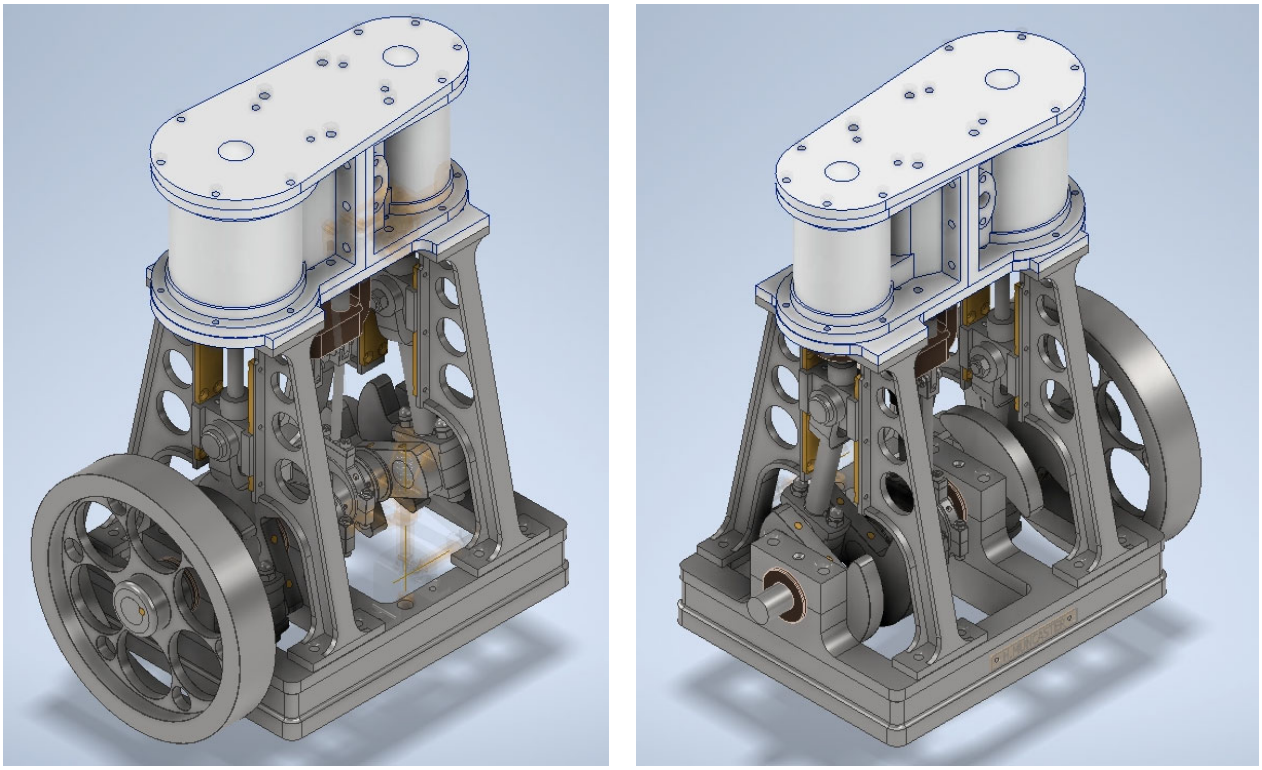

Figure 4. Isometric views of the simplified assembly: front view (**left**) and rear view (**right**).

2.2.2. Assignment of Materials

In this phase, the materials are applied to each of the pieces of the 3D CAD model so that the solid absorbs the mechanical and thermal properties of said material. In the case of the present research, materials from the Autodesk Inventor Professional 2023 material library were assigned. Table 1 shows the materials of the solids that are part of the analysis.

2.2.3. Application of Contacts

Next, the contacts between the different components were established. Autodesk Inventor Nastran 2023 allows the user to set the contacts automatically; however, it set them all to the same type. The types of contact used in this simulation are the following:

- 'Bonded' type: This type of contact represents a welded joint, thus preventing relative movement between the nodes of the meshes of the solids in contact with each other.
- 'Surface' type: This represents the most common contact between two solids. With this type of contact, the relative movement between the nodes of the meshes in contact is allowed. To better understand this type of contact, it can be compared to the sliding of an object on a surface with a certain coefficient of friction.

Table 1. Properties of each material used in the analysis.

Material	Young's Modulus (MPa)	Poisson Coefficient	Density (kg/m^3)	Yield Strength (MPa)
Carbon Steel	200,000	0.290	7850	350.00
Stainless Steel	193,000	0.300	8000	250.00
Cast Iron	120,500	0.300	7150	758.00
Brass	109,600	0.331	8470	103.40
Cast Bronze	109,600	0.335	8870	128.00
Nylon	2930	0.350	1130	82.75
Aluminum 6061	68,900	0.330	2700	275.00

Below, the types of possible penetration are detailed:

- Symmetric contact: The nodes of the mesh of a solid cannot penetrate the mesh of the other solid in contact with it and vice versa.
- Unsymmetrical contact: For this case, the nodes of the mesh of one solid can penetrate the mesh of the opposite solid in contact with it, and vice versa.

In the present investigation, all the contacts have a penetration of the symmetrical type.

Since the coefficient of friction depends on the properties of the materials in contact with each other, as well as the temperature and roughness of the surfaces, a coefficient of friction was established with a value of 0.15 for surfaces in contact with lubrication, and 0.25 for non-lubricated surfaces.

Moreover, the contacts were established automatically by the software and are all of the same 'Bonded' type, being changed manually those of the 'Surface' type, such as the contact of the piston plunger with the cylinder sleeve or that of the friction bearings with the slide shaft, among others.

2.2.4. Boundary Conditions

The boundary conditions consisted of the restriction of the six degrees of freedom of the lower face of the bedplate and the flywheel. In this way, it was possible to simulate the fixing of the steam engine (restricting the underside of the bedplate) and the starting of the engine when it should start the movement (restricting the flywheel). In this way, it was possible to simulate a critical condition, this being the start-up of the machine where it must overcome static coefficients of friction that have values greater than the dynamic coefficients of friction. Therefore, the machine would work in some more critical conditions until movement begins.

Figure 5 shows the restrictions applied to the bedplate and the flywheel.

In a similar manner, in order to better understand the restricted degrees of freedom, the local reference system was drawn for each of the solids, that is, for the bedplate and for the flywheel. This local reference system indicates the direction of the three axes around which the selected surface is prevented from moving or rotating. For the lower surface of the bedplate (Figure 5, left), all the displacements and rotations are prevented. This is because it is necessary to simulate the union of the bedplate to another solid, for example, to the floor of a train. For the flywheel (Figure 5, right), the external surface of the flywheel was prevented since it is necessary to simulate critical positions. In this way, the flywheel lock was simulated (this happens when the machine starts its operation). Nowadays, there are some test benches which measure the torque of modern engines, making it difficult to turn the flywheel. This situation is similar to the one given in the present article. In summary, in both cases, displacements in any direction were prevented, as well as rotation around the axis of the local reference system of each solid.

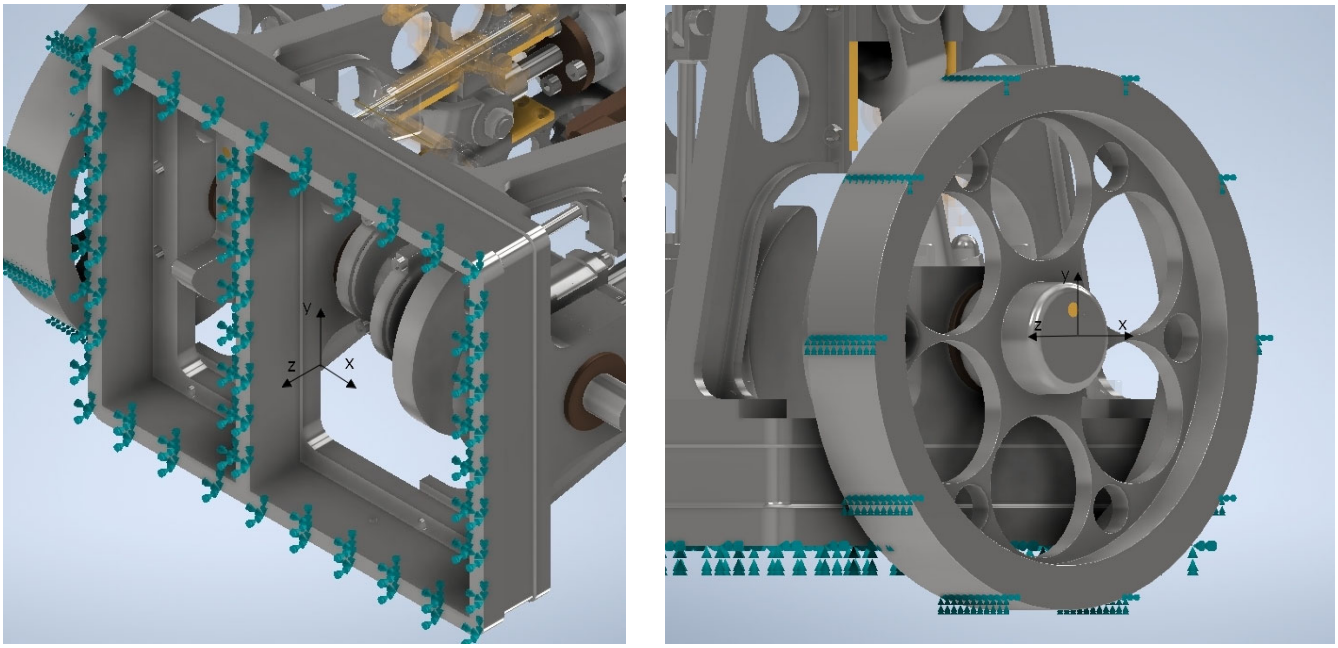

Figure 5. Bedplate fixing (**left**) and flywheel fixing (**right**).

As already mentioned about the reason why the flywheel locks up and based on other previous studies of engine operation [9], the only way for the engine to transfer torque is through the flywheel, since, at the other end of the crankshaft, information on any type of shaft coupling does not exist.

2.2.5. Discretization

Finally, a first global mesh was generated (Figure 6), using second-order interpolation tetrahedral elements. Moreover, the software used (Autodesk Inventor Nastran 2023) automatically refined the mesh in those elements that require a finer grid so that the mesh adapts as well as possible to the geometry of the solid. A maximum element size was established, this being 29 mm. (This is the maximum element size that the software allows us to create, but it is not the size of each one of the elements.) In this way, a mesh of 1,444,410 elements and 2,521,802 nodes was created.

In order to determine the convergence of the mesh and ensure that the results obtained are correct, a refinement was performed in the area of greatest criticality, the area where the maximum values of the von Mises stress are reached. The software allowed this convergence analysis (also called mesh sensitivity analysis) to be performed automatically; however, this process was performed manually, decreasing the size of the finite element in the solids where the critical operating conditions occur. It was decided to carry out this convergence analysis manually in order to obtain a graph with more iterations, given that the software reaches convergence after the second iteration. We were, therefore, able to observe how the mesh converges as the size of the element decreases. Furthermore, mesh convergence in the solution is considered to have occurred when there is a relative error of less than 10% in the von Mises stress between the current iteration (i) and the previous iteration (i-1).

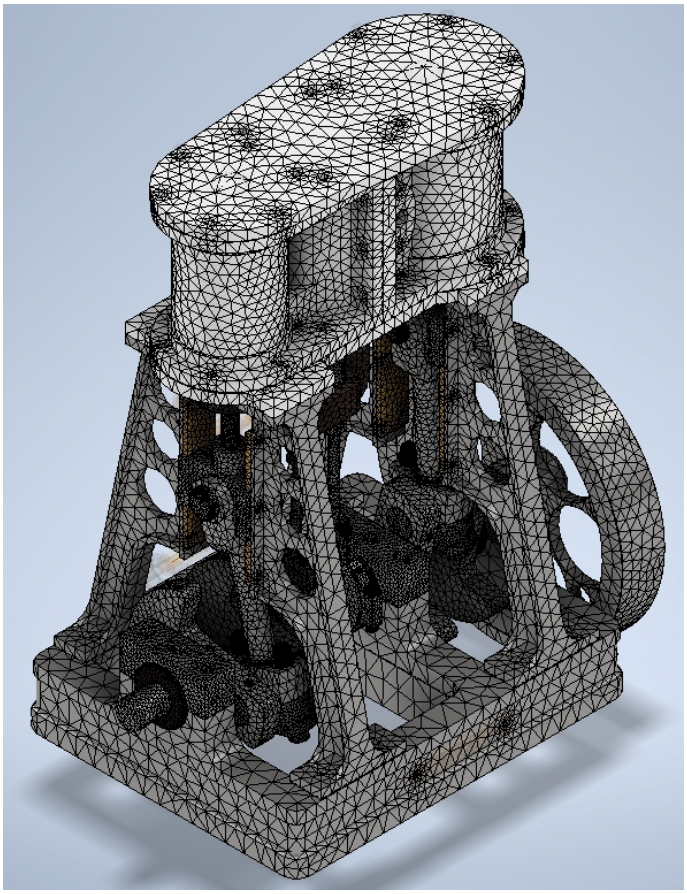

Figure 6. Global mesh.

2.2.6. Critical Positions

There are infinite positions that can be simulated, depending on the angle of rotation of the crankshaft. However, the analysis must be carried out in the critical operating positions, these being when the stresses to which the machine is subjected are at their maximum. For that reason, it is necessary to determine the critical positions, reducing the number of simulations and simulating only those that give rise to the highest value of von Mises stress. In this way, it is possible to determine the maximum values of pressure in the invention, ensuring the operation of the engine under safe conditions. For the present invention, two critical positions were determined:

- Critical position 1: This corresponds to the position of the high-pressure piston plunger in its movement from top dead center to bottom dead center after the intake closes, just when the expansion of the water vapor begins.
- Critical position 2: This corresponds to the position of the high-pressure piston plunger in its displacement from bottom dead center to top dead center after closing the intake, just at the beginning of the expansion of the water vapor.

Figures 7 and 8 show an isometric view and a front view (both sectioned) in each of the critical positions in order to better visualize the position of each of the piston plungers.

2.2.7. Determination of the Strain Envelope

First of all, it is necessary to indicate that there is no information related to the operating conditions of the machine, such as the pressure and temperature of the working fluid (water vapor) in the high-pressure cylinder intake. Therefore, the purpose of this research was to determine the optimal values of the pressure applied to the plunger of each piston, so that the machine works under safe conditions (safety factor greater than unity) under the first-cycle static load.

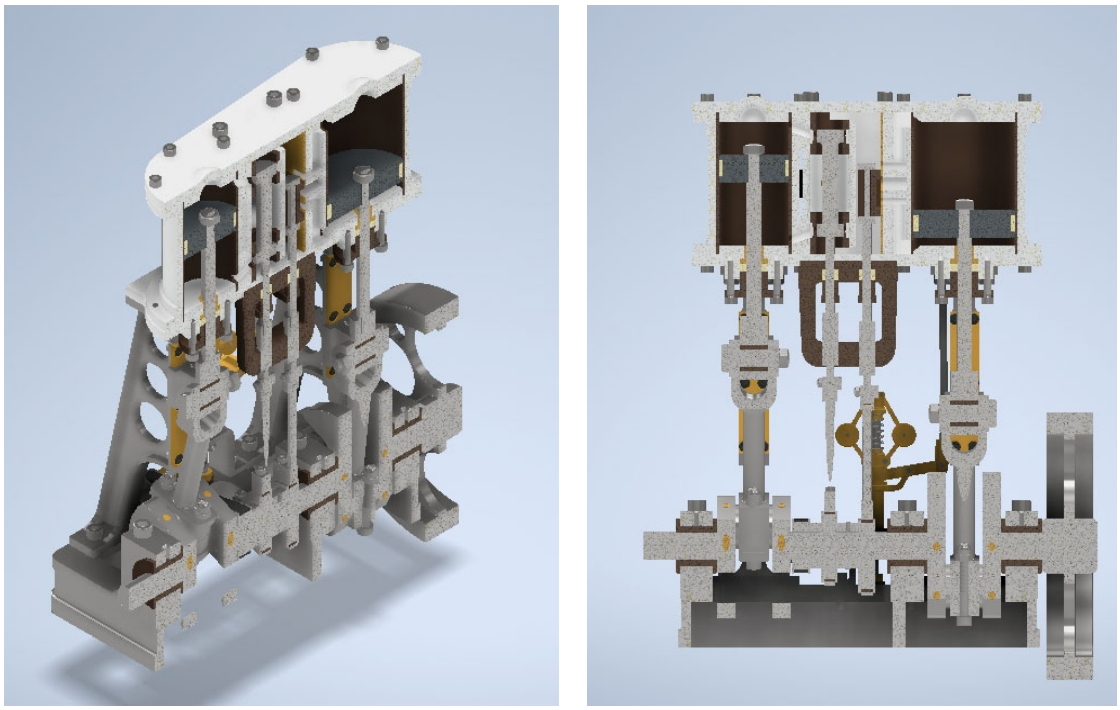

Figure 7. Critical position 1: isometric view (**left**) and front view (**right**).

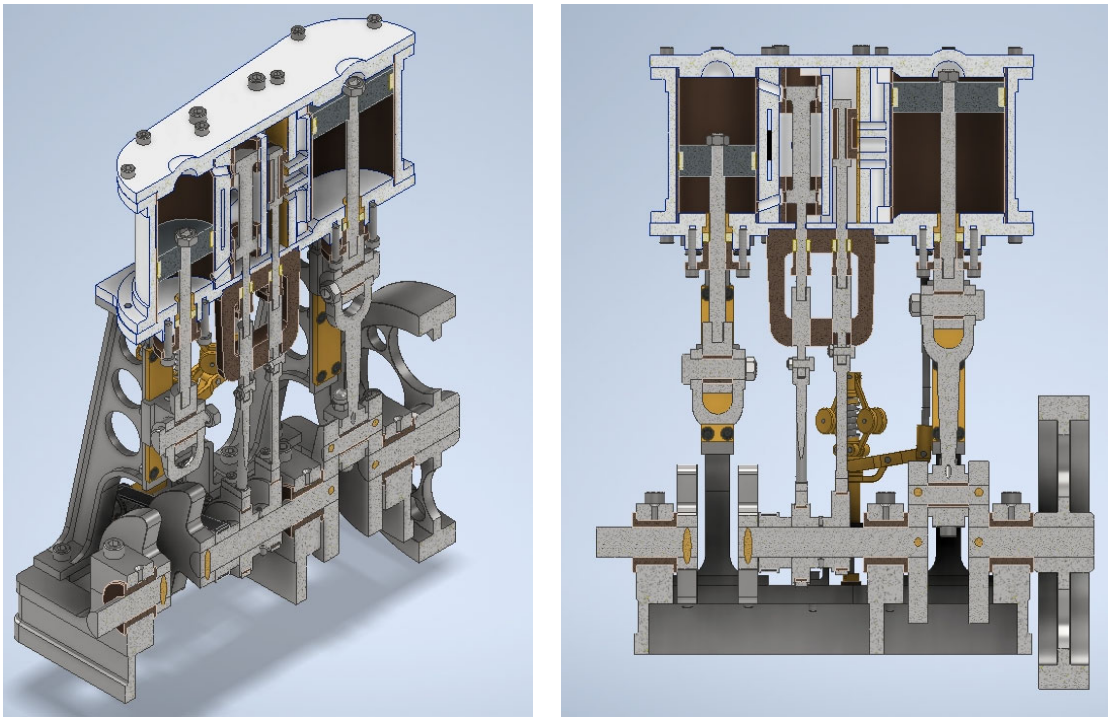

Figure 8. Critical position 2: isometric view (**left**) and front view (**right**).

The difficulty in determining the optimum pressure values is that this machine has two cylinders, a high-pressure and a low-pressure cylinder, so that the pressure at the exhaust of the high-pressure cylinder is the pressure at the intake of the low-pressure cylinder (disregarding possible pressure losses in the intake and exhaust valves, as well as those due to friction). This fact relates the pressure in the cylinders, making it difficult to calculate the pressure applied to the plunger of each piston.

In addition, there is one more unknown factor, which is the angle formed by the eccentric pulley that transmits the rotary movement of the crankshaft to the valves and which has an alternative movement and regulates the intake and exhaust (as explained in Section 2.1). Depending on this angle, the valve closes the intake earlier or later, and, therefore, the expansion of the steam may be one or the other. This is because, if the intake valve closes earlier, the steam expands to reach lower pressure values, and if it closes later, it does not reach such low values after the expansion. Therefore, studying the thermodynamic cycle that occurs inside the cylinder would be the subject of another investigation, since it depends on the aforementioned angle, and determining its optimal value in order to obtain the highest possible thermodynamic performance would be a complex process. Thus, to focus on the objective of this investigation, which was to determine the optimal pressure values so that failure does not occur, some working hypotheses were generated to determine the maximum admissible pressures applied on the faces of the plungers.

The first hypothesis is that, once the pressures on the faces of the plungers are applied with a certain value in order to carry out a first iteration and perform the analysis, the critical area of the greatest von Mises stress cannot be located in an area that both cylinders influence. For example, if, after applying a certain pressure to each of the plungers, it turns out that the von Mises stress is located on the high-pressure piston rod, the value that was applied to the low-pressure cylinder does not matter, since the value of the von Mises stress on the high-pressure piston rod depends only on the pressure applied on the high-pressure cylinder and not on the low-pressure one. This hypothesis allows different iterations to be carried out so that, while this hypothesis is fulfilled, pressures can be applied to the plungers, and their value can be modified until the entire machine complies (that is, a safety factor is obtained for all of it that is greater than unity).

On the other hand, if the von Mises stress is located in an area where both plungers have influence, for example, in some area of the crankshaft, the previous hypothesis cannot be applied, and it would be necessary to determine the water vapor pressure after the expansion in the high-pressure cylinder in order to obtain the value of the vapor pressure at the intake of the low-pressure cylinder.

Therefore, and to finish with this section, the process carried out to determine the optimal pressure values is explained here. In the first place, it is necessary to highlight that the maximum admissible pressure value in the high-pressure piston plunger is the result of the difference between the intake pressure in this cylinder and the exhaust pressure, since as the steam does not fully expand, on the opposite side of the plunger, there is also an applied pressure (exhaust), and, therefore, the calculated pressure in the high-pressure cylinder is the difference in pressure. As for the low-pressure cylinder, the pressure calculated for it is the maximum admissible pressure in the admission of the low-pressure cylinder, this being the manometric pressure, since the steam fully expands up to atmospheric pressure, and on the opposite face of the plunger, pressure is applied whose value is the atmospheric pressure.

A first analysis was carried out with a high value of pressure applied to both pistons. After carrying out this first simulation, it was possible to observe whether or not the previously described hypothesis was fulfilled. If so, the distribution of the safety factor in the machine is shown. Different simulations were carried out in this way, modifying the value of the pressure applied until the optimal values were obtained based on the values of the safety factor.

In Figures 9 and 10, we can see the application of the pressure load for each critical position.

Actually, there are pressure loads applied to the cylinder walls, including the top and bottom cylinder decks. However, since the cylinders and platforms are oversized, the value of the von Mises stress caused by pressure applied to the walls of each cylinder is very small compared to the von Mises stress caused by pressure applied to the corresponding face of each piston plunger. Therefore, to simplify the analysis and reduce the calculation time, the pressure loads applied to the cylinder walls can be neglected.

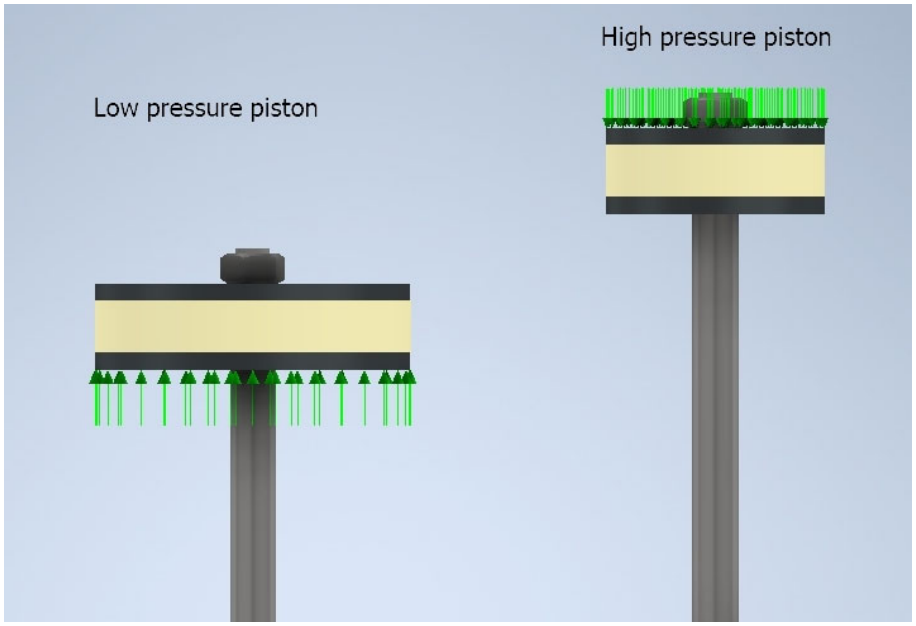

Figure 9. Application of loads for critical position 1.

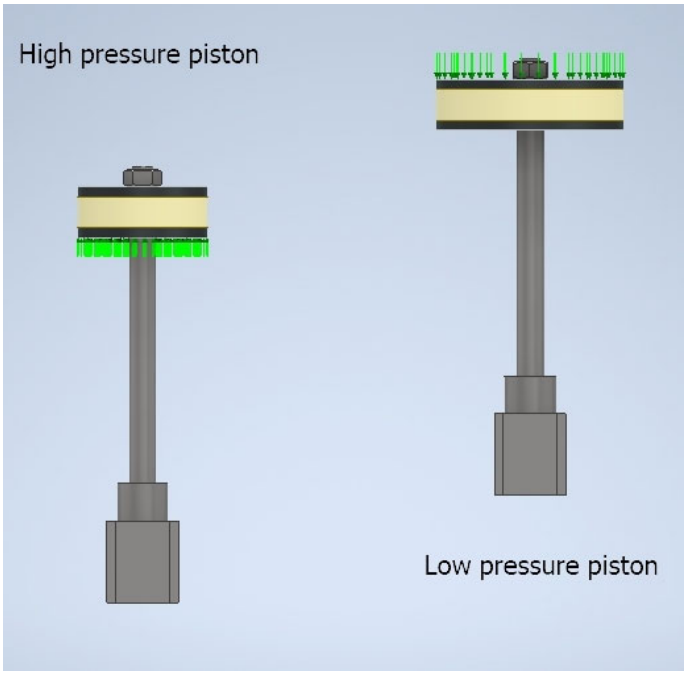

Figure 10. Application of loads for critical position 2.

2.2.8. Analysis Execution

Modal Analysis

Before performing a static linear analysis, it is necessary to determine the first natural frequencies of vibration for each critical position. In a modal analysis, the natural frequencies of vibration can be determined for each mode of vibration, the mode of vibration being the deformation experienced by the system (in this case the steam engine) for a given frequency and this being the natural frequency of vibration.

In this way, it is possible to determine if the steam engine behaves like a mechanism or not for a given position. If the system does not behave like a mechanism, it makes sense to carry out a static linear analysis, since the first two natural frequencies of vibration are

greater than zero, thus indicating that the resonance phenomenon that would imply large displacements and/or deformations does not occur.

Therefore, in the present research, the first ten natural frequencies of vibration were determined (although only two of them are necessary), and we verified that they were greater than zero so that it made sense to carry out a subsequent static linear analysis.

The system initially was a one-degree-of-freedom mechanism, but a boundary condition was set, fixing the flywheel, so the motion of the whole system was stopped. With those boundary conditions, the system behaved as a structure, and obviously a static analysis was allowed, without the need of checking it with a modal analysis. Nevertheless, a modal analysis is required to know the natural frequencies of the steam engine since the velocity of rotation of the crankshaft is limited to certain values, avoiding said natural frequencies and, therefore, the resonance of the system, what would lead to a bad functioning of the engine.

Static Linear Analysis

After the modal analysis, a static linear analysis was carried out in order to determine the optimal working pressures of the machine under first-cycle static load. Thus, the value that each of the variables took was observed, that is, the von Mises stress, the displacement and the safety factor.

The safety factor is obtained by dividing the yield strength of the material by the von Mises stress at a given point. If this factor is greater than unity in the entire machine, then the machine works under safe conditions, taking as a failure criterion the plasticization of a cross-section of some solid component.

Von Mises stress is a good criterion to compare it with yield strength because it is a physical magnitude that is proportional to distortion energy. It is a good failed criterion for ductile materials because, according to Richard Edler von Mises, a ductile material fails when distortion energy reaches a determinate value.

For this reason, a static linear analysis was performed to find out if any element of the machine plasticized because a permanent deformation caused it to malfunction, giving rise to an increase in vibrations, possible pressure losses in the cylinders and many other negative effects that permanent deformations (also called plastic deformations) would entail.

3. Results and Discussion

This section shows the results obtained for each of the critical positions studied. Before presenting of the results, it should be noted that the figures corresponding to the von Mises stresses' distribution, displacements and safety factor are screenshots from the Autodesk Inventor Nastran 2023 software, where the decimal separator used is the comma and not the dot.

3.1. Modal Analysis

3.1.1. Critical Position 1

Figure 11 shows the graph with the natural vibration frequency associated with each vibration mode, and Table 2 shows the values of these frequencies. As can be seen, the natural vibration frequencies associated with the first ten modes of vibration are greater than zero, and, therefore, the steam engine does not behave as a mechanism for the critical position 1, so it makes sense to perform a static linear analysis for that position.

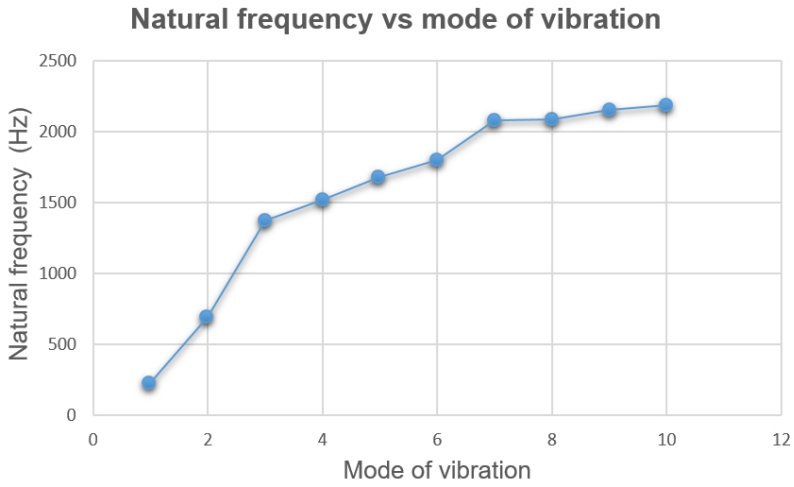

Figure 11. Natural frequency vs. mode of vibration.

Table 2. Values of the natural frequency for each mode of vibration.

Mode of Vibration	Natural Frequency (Hz)
1	222.856
2	690.978
3	1371.334
4	1520.094
5	1678.204
6	1799.994
7	2078.845
8	2089.351
9	2155.662
10	2189.124

3.1.2. Critical Position 2

The same procedure was followed for critical position 2. Figure 12 shows the graph with the natural frequency of vibration associated with each mode of vibration, and Table 3 shows with the values of the natural frequencies.

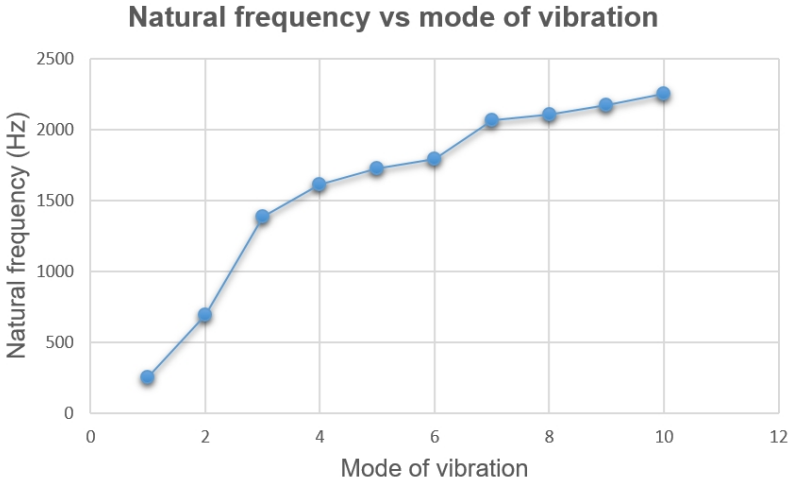

Figure 12. Natural frequency vs. mode of vibration.

Table 3. Values of the natural frequency for each mode of vibration.

Mode of Vibration	Natural Frequency (Hz)
1	256.206
2	691.678
3	1386.978
4	1614.984
5	1725.334
6	1793.178
7	2064.468
8	2105.807
9	2172.460
10	2256.000

As can be seen, the natural vibration frequencies associated with the first ten modes of vibration are greater than zero, and therefore the steam engine does not behave as a mechanism for the critical position 2, so it makes sense to carry out a static linear analysis for that position.

3.2. Static Linear Analysis

The results obtained in the static linear analysis for each of the critical positions are shown below. First, the von Mises stress distribution is shown for a high-pressure value (first iteration), and we determined in which component its highest value is located. In addition, the previously explained hypothesis (Section 2.2.7) was confirmed, which would allow us to work with both cylinders independently when pressure is applied to the piston of each cylinder. Moreover, the results obtained (von Mises stress distribution, displacements and safety factor) are shown for the maximum allowable working pressures.

3.2.1. Critical Position 1

In the first place, an analysis was carried out by applying a pressure of a value of 0.65 MPa in both pistons in order to observe the distribution of von Mises stresses and the safety factor and so determine how the machine behaves for a high-pressure value and determine, in a first estimate, the most critical area, thus confirming or negating the hypothesis.

Figures 13 and 14 show the von Mises stress distribution and the safety factor distribution, respectively.

After this first analysis (pressure of 0.65 MPa) it can be observed that the maximum values of the von Mises stress are located on the surface of the rod cap of both pistons; therefore, compliance with the aforementioned hypothesis is confirmed, also noting that the safety factor is greater than unity.

However, paying attention to this safety factor and reaching the conclusion that the pressure value applied would be optimal would be a mistake, since these results were obtained for a first mesh, without carrying out a convergence analysis, that is, without performing a mesh refinement in the most critical areas. Similarly, it was verified that if a refinement of the mesh were carried out, the value of the von Mises stress would increase, and a safety factor of less than unity would be obtained.

Thus, since the working hypothesis was confirmed, independent pressure values can be applied to the plunger of each one of the pistons. In this way, after carrying out several simulations, the maximum admissible pressure values were obtained: 0.3 MPa in the high-pressure piston plunger and 0.15 MPa in the low-pressure piston plunger. Additionally, the pressure applied to the piston plunger is the difference between the maximum admissible pressure difference and that determined in the low-pressure cylinder, that is, the maximum admissible in the low-pressure cylinder intake, this being manometric.

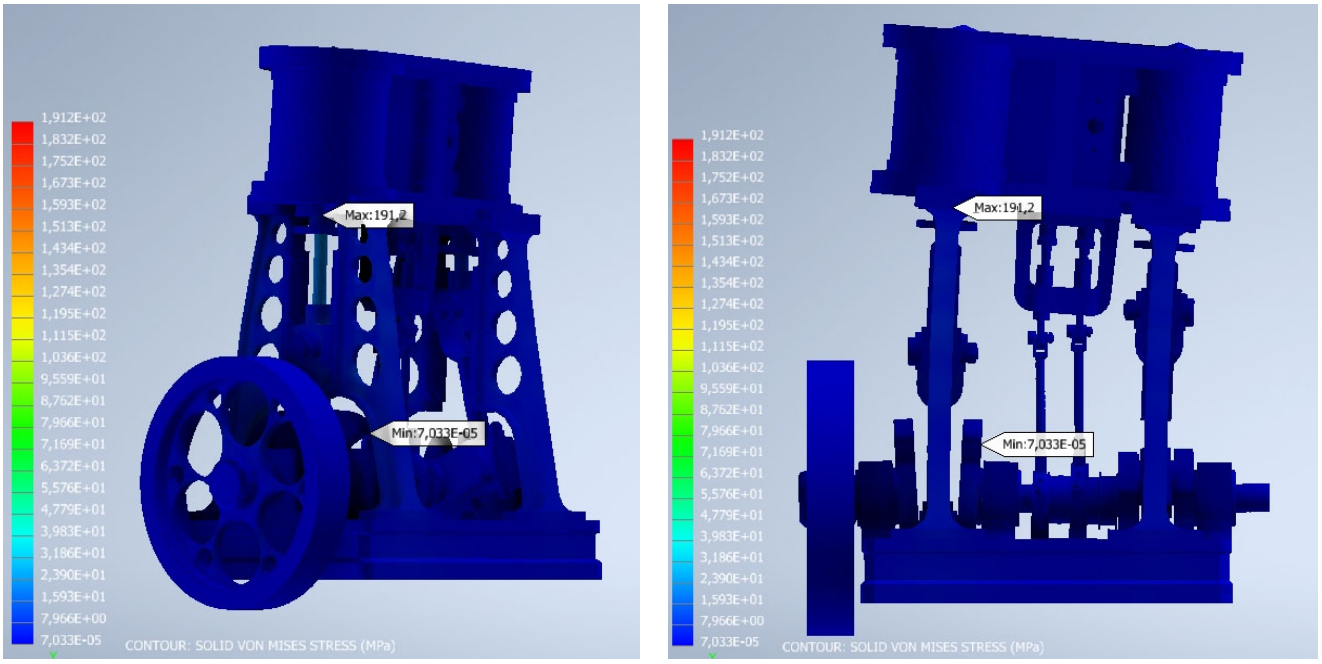

Figure 13. Von Mises stress distribution: isometric view (**left**) and location of the highest value (**right**).

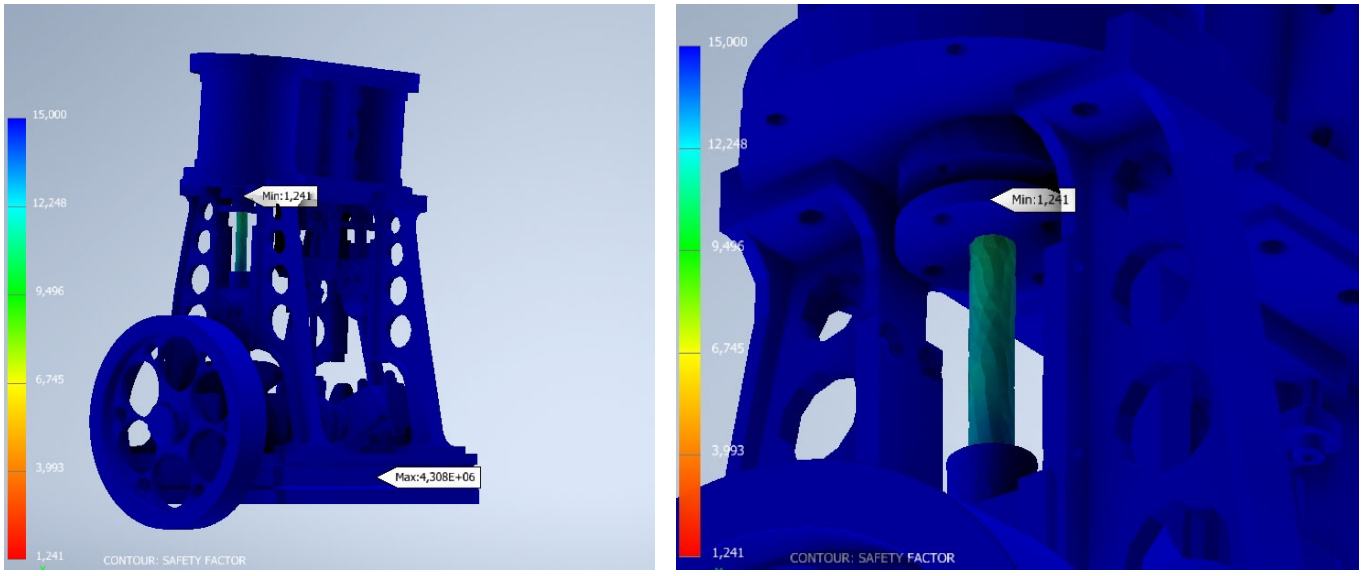

Figure 14. Safety factor distribution: isometric view (**left**) and location of the lowest value (**right**).

Finally, Figure 15 shows the convergence analysis of the mesh, and Table 4 shows the values of the mesh size of the refined elements, the iteration number, the von Mises stress and the relative error obtained.

As can be seen, the relative error obtained is 0.64% in the fourth iteration, that is, a negligible error and less than 10%; therefore, it can be concluded that the mesh converges in this iteration.

Figure 16 shows the distribution of the von Mises stress in the assembly for the maximum admissible pressure values indicated previously, where it can be seen that the maximum von Mises stress is located in the high-pressure piston rod cap, with a value of 96.57 MPa.

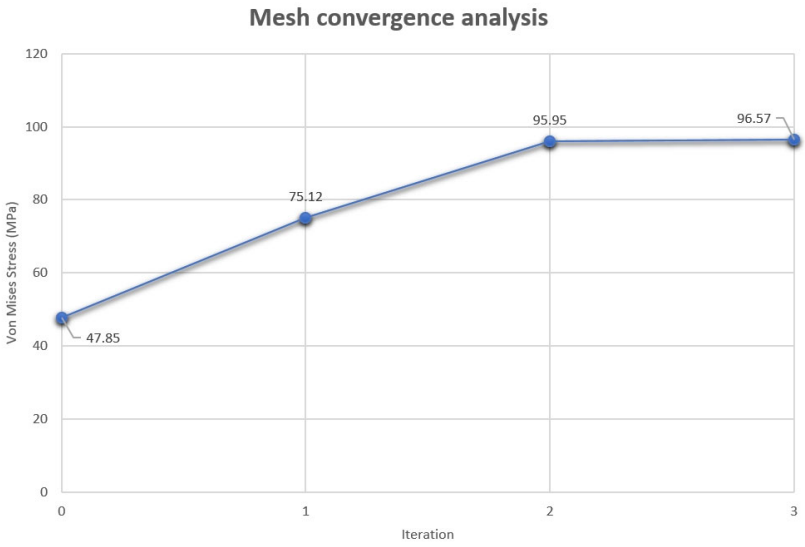

Figure 15. Mesh convergence analysis graph.

Table 4. Mesh convergence analysis data.

High-Pressure Piston Rod Cap Element Size (mm)	High-Pressure Piston Rod Cap Element Size (mm)	Iteration	Von Mises Stress (MPa)	Relative Error (%)
0.75	2.75	0	47.85	-
0.45	1.25	1	75.12	36.30
0.425	1.125	2	95.95	21.71
0.38	0.9	3	96.57	0.64

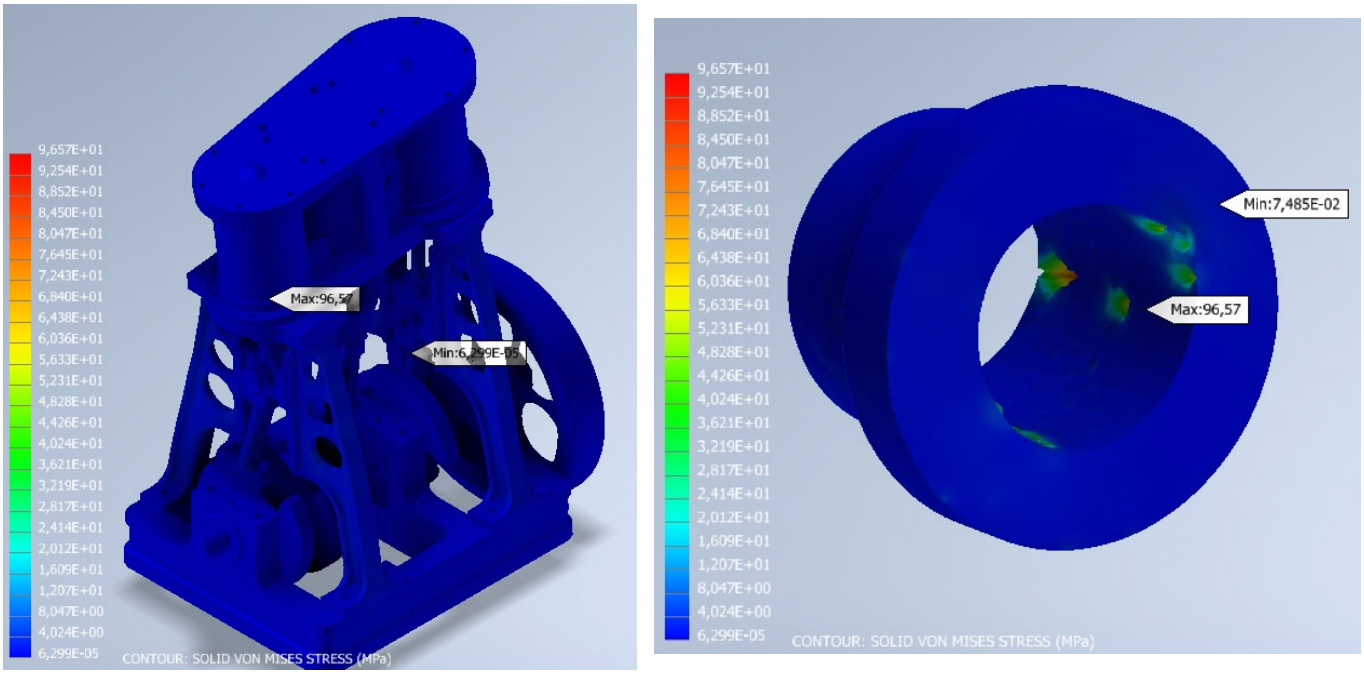

Figure 16. Von Mises stress distribution (**left**) and location of the highest value (**right**).

Similarly, Figure 17 shows the distribution of the displacements, where the displacements are displayed with a magnification factor of 10 in order to observe the deformed position of the machine more clearly. As can be seen, the maximum displacement has a value of 4.106×10^{-3} mm in the high-pressure piston plunger, this being a negligible value.

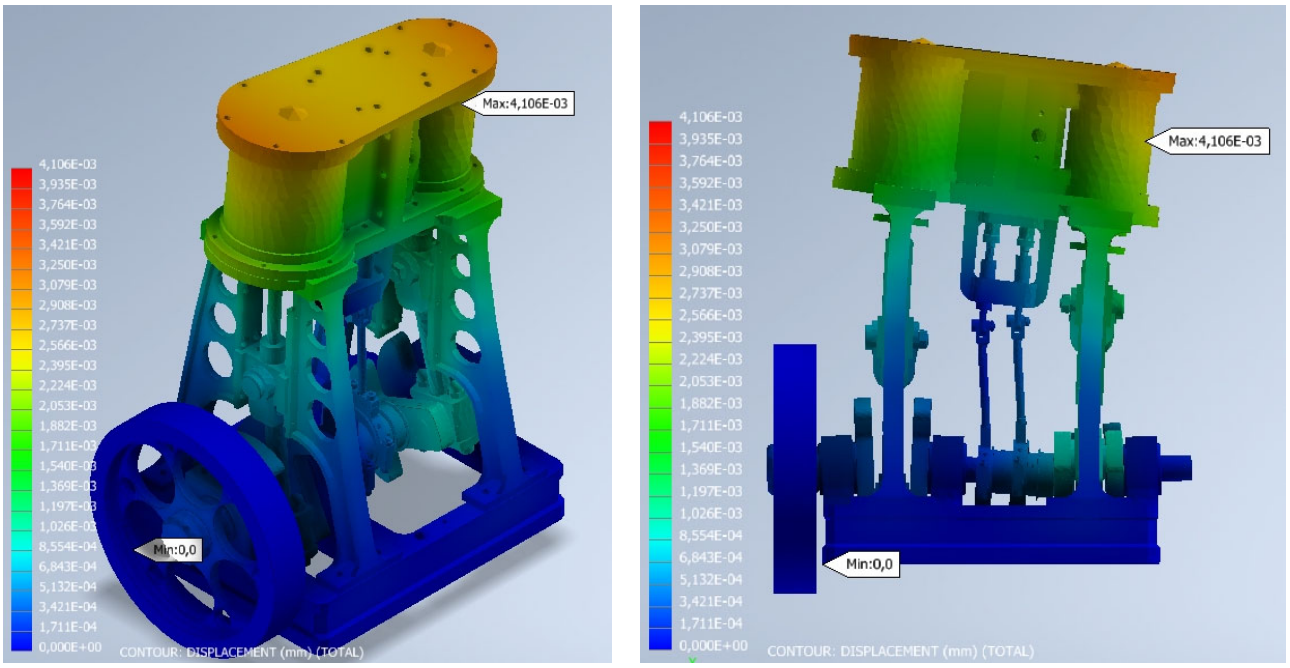

Figure 17. Displacement distribution: isometric view (**left**) and front view (**right**).

Finally, Figure 18 shows the distribution of the safety factor. Thus, the minimum value of the safety factor is located in the high-pressure piston rod cap, with a value of 1.785, greater than unity. Therefore, it can be confirmed that the pressures applied are the maximum admissible values for the failure criterion for static load of the first cycle, since they offer a safety factor greater than unity.

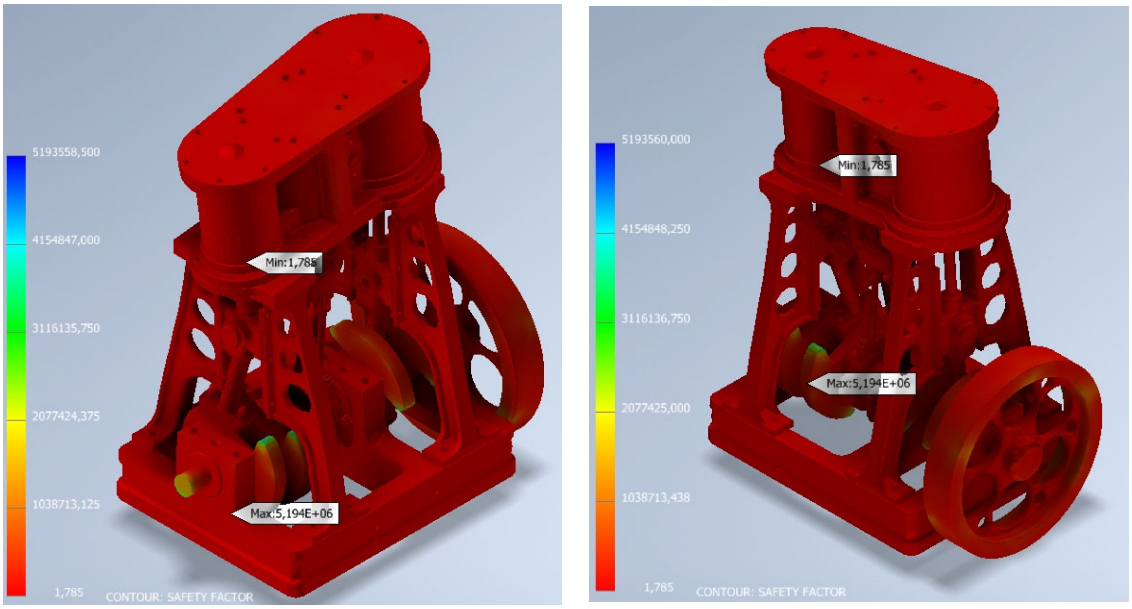

Figure 18. Safety factor distribution: rear isometric view (**left**) and front isometric view (**right**).

3.2.2. Critical Position 2

In this case, and unlike critical position 1, the maximum admissible pressure values for each piston are already available, so it is only necessary to confirm that these values also comply with this position, that is, that the safety factor is also greater than unity.

Figure 19 shows the mesh convergence analysis, and Table 5 shows the mesh size value for each iteration in the most critical elements, the von Mises stress obtained in each iteration and the resulting relative error.

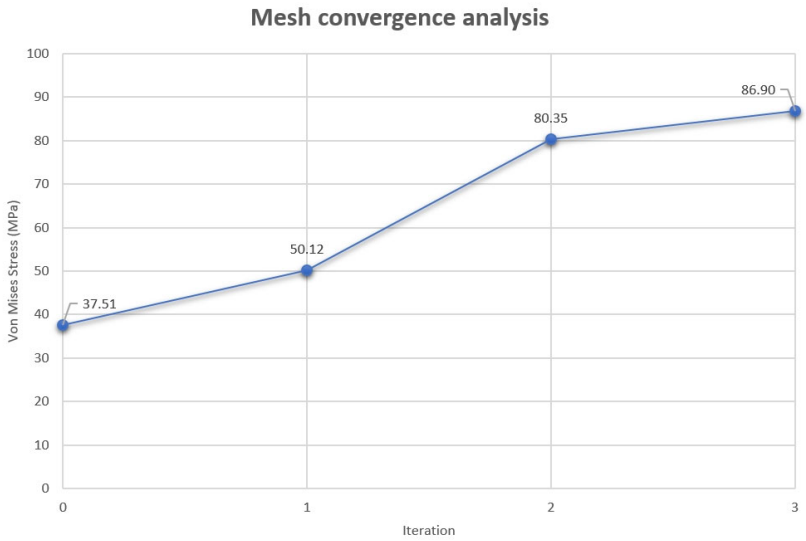

Figure 19. Mesh convergence analysis graph.

Table 5. Mesh convergence analysis data.

High-Pressure Piston Rod Cap Element Size (mm)	High-Pressure Piston Rod Cap Element Size (mm)	Iteration	Von Mises Stress (MPa)	Relative Error (%)
0.88	3.90	0	37.51	-
0.60	2	1	50.12	25.16
0.40	1.25	2	80.35	37.62
0.38	1.15	3	86.90	7.53

On this occasion, and for this critical position, the convergence of the mesh was reached in the fourth iteration, obtaining a relative error of 7.53%, less than 10%. Therefore, it can be affirmed that the mesh converges.

In Figure 20, the von Mises stress distribution is shown. As can be seen, the maximum von Mises stress is located in the high-pressure piston rod cap, with a value of 86.9 MPa.

Figure 21 shows the distribution of displacements in mm, with an enlargement factor of 10 in order to observe the deformed position of the machine more clearly. As can be seen, the maximum displacement occurs in the plunger of the high-pressure piston, with a value of 4.851×10^{-3} mm, this being practically negligible.

Finally, Figure 22 shows the distribution of the safety factor, noting that the minimum safety factor is located in the high-pressure piston rod cap, with a value of 2.102, which is greater than unity.

3.3. Discussion of the Results

After carrying out different analyses, with different pressure values, the maximum admissible values were determined: 0.3 MPa in the high-pressure piston plunger and 0.15 MPa in the low-pressure piston plunger. Since the steam does not fully expand in the high-pressure cylinder, this would mean a pressure corresponding to the value of the vapor pressure on the opposite side after expansion. For this reason, the value obtained (0.3 MPa) is the maximum admissible pressure difference in the high-pressure cylinder. This is the value resulting from the difference between the intake pressure of the cylinder and the exhaust pressure, the steam pressure after the first expansion. As an example, if the pressure after expansion acquires a value of 0.15 MPa, then the maximum allowable pressure at the

intake of the high-pressure cylinder is 0.45 MPa (0.3 + 0.15), since the maximum difference allowable is 0.3 MPa, which is the calculated value. Similarly, the value of the maximum admissible pressure in the low-pressure cylinder is 0.15 MPa, this being a manometric pressure value given that the steam is expelled at atmospheric pressure.

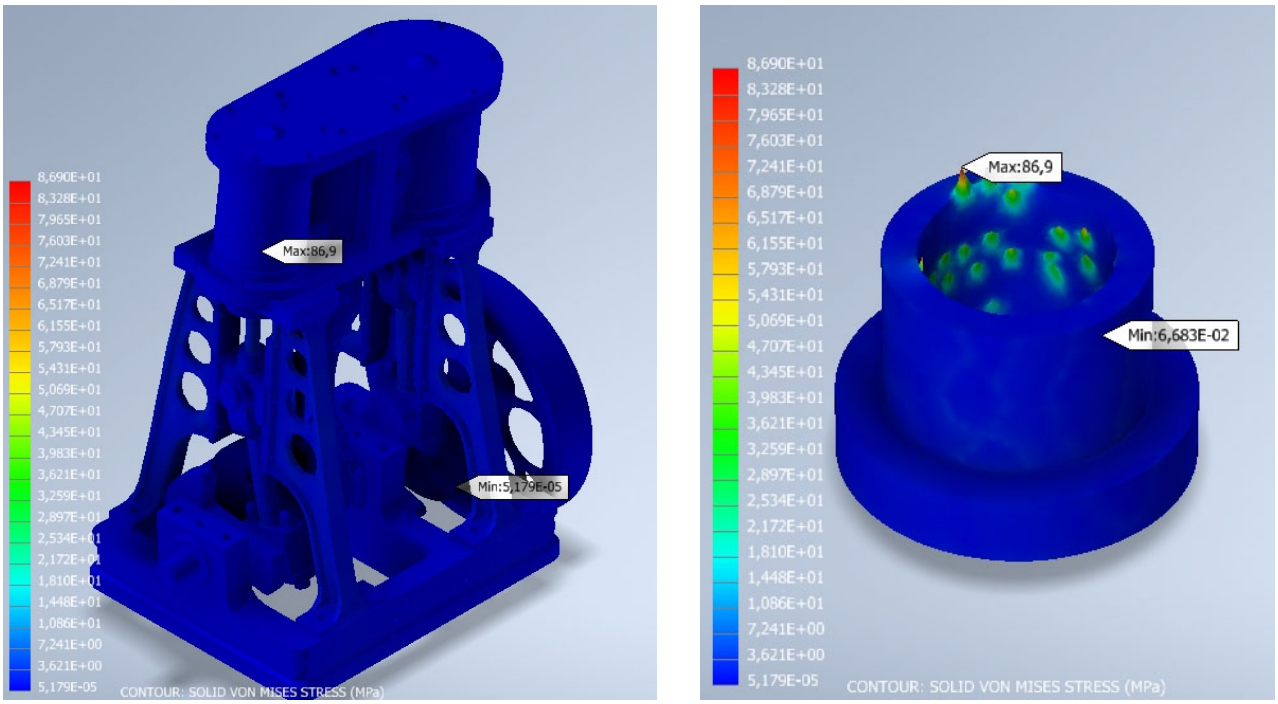

Figure 20. Von Mises stress distribution (**left**) and location of the highest value (**right**).

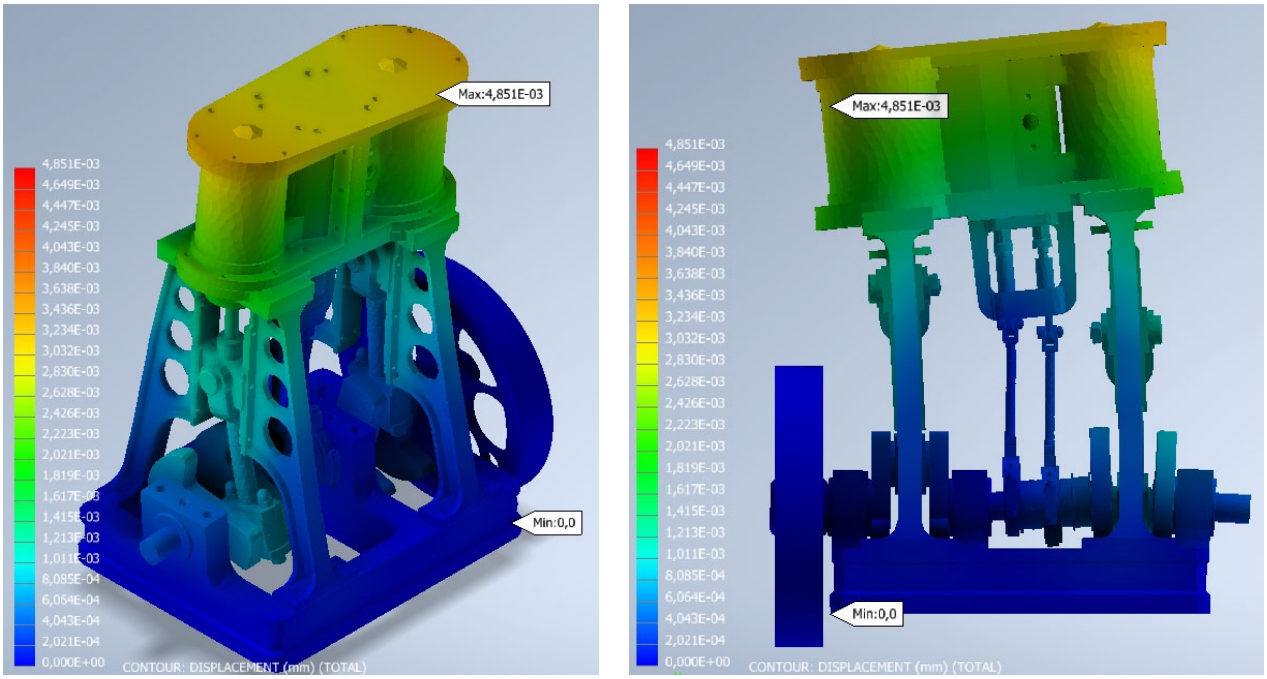

Figure 21. Displacement distribution: isometric view (**left**) and front view (**right**).

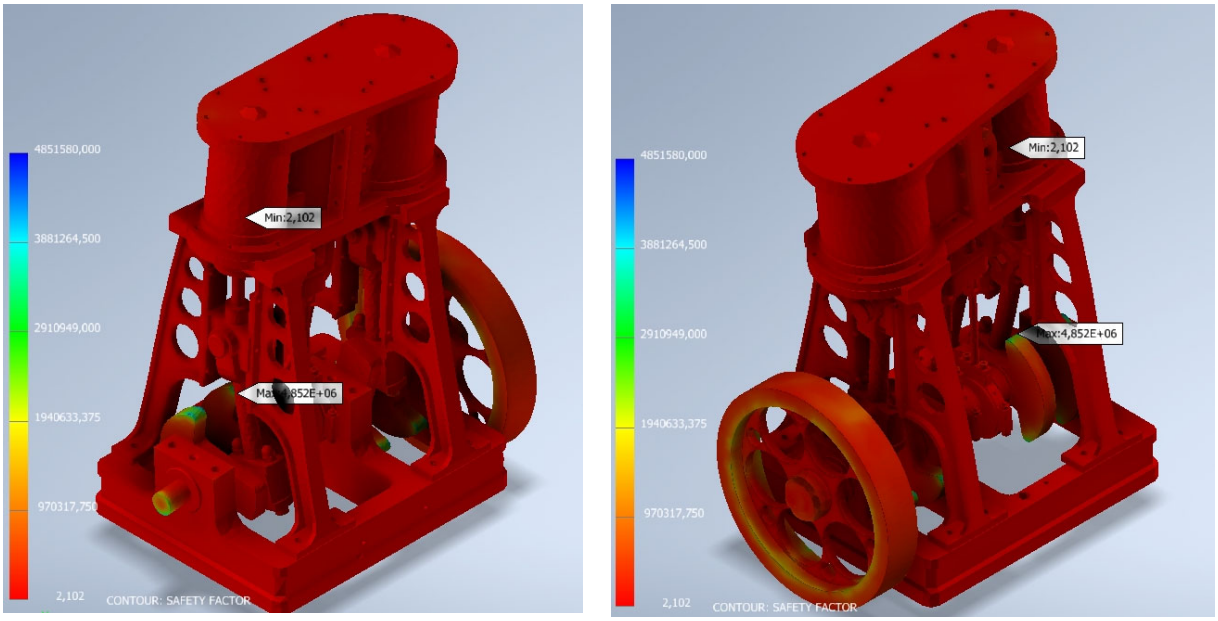

Figure 22. Safety factor distribution: rear isometric view (**left**) and front isometric view (**right**).

Therefore, these are the values that offer the operation of the machine under safe conditions, with the failure criterion applied being the reach of the yield strength under the static load of the first cycle for the situation of blocking the flywheel in the start-up of the machine as the most unfavorable situation.

Finally, to summarize the results obtained, Tables 6 and 7 show the maximum values of stress and displacement, as well as the minimum value of the safety factor, for each critical position.

Table 6. Results for critical position 1.

Variable	Value
Von Mises stress (maximum value; MPa)	96.57
Displacement (maximum value; mm)	4.106×10^{-3}
Safety factor (minimum value)	1.785

Table 7. Results for critical position 2.

Variable	Value
Von Mises stress (maximum value; MPa)	86.90
Displacement (maximum value; mm)	4.851×10^{-3}
Safety factor (minimum value)	2.102

4. Conclusions

In this paper, a two-cylinder compound vertical steam engine with speed control designed by Henry Muncaster was analyzed in order to obtain the maximum admissible operating conditions according to the criteria of the resistance of materials, in particular, under failure by first-cycle static load (limit of the yield strength of the material). This means that permanent deformations were not allowed for the determination of the operating conditions.

As there is no information on the operating conditions (pressure), the purpose of this investigation was their determination. The estimated conditions for the safe operation of the machine were the maximum admissible pressure difference in the high-pressure cylinder and the maximum admissible pressure in the low-pressure cylinder intake. The

pressure difference in the high-pressure cylinder corresponds to the difference between the intake pressure value and the exhaust pressure value, i.e., the pressure of the fluid after expansion. In this way, by simulating two critical operating conditions that resemble the start-up of the machine (flywheel locked as the most unfavorable situation), the operating conditions were determined which ensure both its safety and its optimal functioning, since the appearance of plastic deformations of some components of the machine could give rise to an increase in vibrations or pressure losses in the chambers of the cylinders or valves, among other consequences.

On the other hand, for critical position 1 (corresponding to the movement of the piston plunger from top dead center to bottom dead center after the intake is closed), different simulations were carried out to determine the optimal operating conditions. These conditions were a maximum allowable pressure difference in the high-pressure cylinder of 0.3 MPa and a maximum allowable pressure in the low-pressure cylinder intake of 0.15 MPa. For these conditions, and for a relative error in the mesh convergence analysis of 0.64% in the fourth iteration, a maximum von Mises stress of 96.57 MPa is obtained in the high-pressure piston rod cap, a maximum displacement of 4.106×10^{-3} mm on the high-pressure piston plunger and a minimum safety factor of 1.785 on the high-pressure piston rod cap.

We proceeded in a similar way for critical position 2 (corresponding to the displacement of the high-pressure piston plunger from bottom dead center to top dead center after closing the intake); however, the operating conditions for this critical position were known because they were already determined for critical position 1. In this case, it would only be verified that the machine also complies with these operating conditions, that is, that the lowest safety factor is also greater than unity. After performing a mesh convergence analysis, a relative error of 7.53% was obtained in the fourth iteration, as well as a maximum von Mises stress of 86.9 MPa in the high-pressure piston rod cap, a maximum displacement of 4.851×10^{-3} mm on the low-pressure piston plunger and a minimum safety factor of 2.102 on the high-pressure piston rod cap.

As possible future research, as the dimensions of the machine in the plans [9] are small and this machine could be installed in small boats or railways, a dimensional analysis could be carried out that relates dimensional parameters and operating conditions in order to determine the appropriate dimensions that this machine should have in order to obtain an effective performance.

In addition, in the invention, there is an eccentric pulley that regulates the reciprocating movement of the valves, and this forms an angle with the crankshaft axis. Thus, depending on the angle, the valves close sooner or later, modifying the thermodynamic cycle carried out by the water vapor inside the cylinders. For this reason, it is proposed to carry out an analysis of this thermodynamic cycle in order to determine the optimal angle formed by the eccentric pulley with the crankshaft axis, the one that offers the best thermodynamic performance of the cycle.

Author Contributions: Conceptualization, J.I.R.-S.; methodology, J.I.R.-S. and J.F.G.-A.; investigation, J.I.R.-S. and J.F.G.-A.; formal analysis, J.I.R.-S. and J.F.G.-A.; visualization, J.I.R.-S. and J.F.G.-A.; supervision, J.I.R.-S.; writing—original draft preparation, J.I.R.-S. and J.F.G.-A.; writing—review and editing, J.I.R.-S. and J.F.G.-A. All authors have read and agreed to the published version of the manuscript.

Funding: The research presented in this paper was possible thanks to a collaboration grant with the Department of Engineering Graphics, Design and Projects of the University of Jaen obtained in the 2022 call from the Ministry of Education and Vocational Training of the Government of Spain.

Institutional Review Board Statement: Not applicable.

Informed Consent Statement: Not applicable.

Data Availability Statement: Not applicable.

Acknowledgments: We would like to thank the anonymous reviewers of this paper for their constructive suggestions and comments.

Conflicts of Interest: The authors declare no conflict of interest.

References

1. Inkster, I. (Ed.) *History of Technology*; Bloomsbury Academic: London, UK, 2004; Volume 25.
2. Jenkins, R. *Links in the History of Engineering and Technology from Tudor Times*; The Newcomen Society at the Cambridge University Press: Cambridge, UK, 1971.
3. Russell, B. *James Watt: Making the World Anew*; Reaktion Books: London, UK, 2014.
4. Rojas-Sola, J.I.; Galán-Moral, B.; De la Morena-de la Fuente, E. Agustín de Betancourt's double-acting steam engine: Geometric modeling and virtual reconstruction. *Symmetry* **2018**, *10*, 351. [CrossRef]
5. Rojas-Sola, J.I.; De la Morena-de la Fuente, E. Agustín de Betancourt's double-acting steam engine: Analysis through computer-aided engineering. *Appl. Sci.* **2018**, *8*, 2309. [CrossRef]
6. Who Was Henry Muncaster? Available online: https://modelengineeringwebsite.com/Henry_Muncaster.html (accessed on 13 July 2023).
7. Muncaster, H. *Model Stationary Engines—Their Design and Construction*; TEE Publishing Ltd.: Oxford, UK, 1912.
8. Rojas-Sola, J.I.; Gutiérrez-Antúnez, J.F. Analysis of the design of the single-cylinder steam engine of the grasshopper beam by Henry Muncaster. *Machines* **2023**, *11*, 703. [CrossRef]
9. Rojas-Sola, J.I.; Gutiérrez-Antúnez, J.F. Geometric modeling and digital restitution of a two-cylinder compound vertical steam engine with speed control by Henry Muncaster. In *Advances in Engineering Design IV*, 1st ed.; Accepted for Publication; Manchado del Val, C., Suffo Pino, M., Miralbés Buil, R., Moreno Sánchez, D., Moreno Nieto, F.D., Eds.; Springer: Cham, Switzerland, 2024.
10. Two-Cylinder Compound Vertical Marine Engine. Available online: https://modelengineeringwebsite.com/Muncaster_compound.html (accessed on 13 July 2023).
11. Edgar, T. Westbury. Available online: https://en.wikipedia.org/wiki/Edgar_T._Westbury (accessed on 13 July 2023).
12. Liu, Y.; Huang, M.; An, Q.; Bai, L.; Shang, D.Y. Dynamic characteristic analysis and structural optimization design of the large mining headrame. *Machines* **2022**, *10*, 510. [CrossRef]
13. Stavroulakis, G.E.; Charalambidi, B.G.; Koutsianitis, P. Review of computational mechanics, optimization, and machine learning tools for digital twins applied to infrastructures. *Appl. Sci.* **2022**, *12*, 11997. [CrossRef]
14. Jumper, L.; Shih, R.H. *Parametric Modeling with Autodesk Inventor 2023*; SDC Publications: Mission, KS, USA, 2022.
15. Autodesk Inventor Nastran 2023. About Tutorials. Available online: https://help.autodesk.com/view/NINCAD/2023/ENU/?guid=GUID-DB7160BE-0C72-47B9-B5EF-FC4925B455CE (accessed on 13 July 2023).